Calculating energy loss spectra of NiO: Advantages of the modified Becke-Johnson potential

Walid Hetaba,[1,*] Peter Blaha,[2] Fabien Tran,[2] and Peter Schattschneider[1,3]

[1]*Institute of Solid State Physics, Vienna University of Technology, Wiedner Hauptstraße 8-10/138, A-1040 Vienna, Austria*

[2]*Institute of Materials Chemistry, Vienna University of Technology, Getreidemarkt 9/165-TC, A-1060 Vienna, Austria*

[3]*University Service Center for Transmission Electron Microscopy, Vienna University of Technology, Wiedner Hauptstraße 8-10/052, A-1040 Vienna, Austria*

(Received 5 January 2012; published 7 May 2012)

The density of states and the energy loss near-edge structure of the oxygen K edge in NiO are calculated using different models for the exchange-correlation functional. The results are compared to each other and to experimentally acquired energy loss spectra. It is found that only when using the modified Becke-Johnson potential are the calculated spectra in good agreement with the experimental data. This can be achieved at much less computational costs than with more sophisticated calculation methods but with as good results.

DOI: 10.1103/PhysRevB.85.205108 PACS number(s): 71.15.Mb, 71.20.Be, 79.20.Uv

I. INTRODUCTION

Currently, simulations are often necessary in analytical transmission electron microscopy (TEM) to interpret experimental data. Electron energy loss spectrometry (EELS) is a commonly used method in analytical TEM that measures the kinetic energy of the probe electrons after the interaction with the sample.[1,2] The resulting spectra show distinct peaks resulting from core excitations. These peaks exhibit a fine structure which is called energy loss near-edge structure (ELNES). It reflects the chemical composition and electronic structure in the surrounding of the excited atom. Calculations of the ELNES are usually performed by means of *ab initio* methods. One largely used possibility is to utilize software packages based on density functional theory (DFT)[3] and the Kohn-Sham equation.[4] The crucial point of these calculations is to describe the exchange-correlation effects as accurately as possible. Which particular method for the exchange-correlation effects gives acceptable results depends strongly on the investigated material and on the desired property.

Although the local-density approximation (LDA)[5] or the generalized gradient approximation (GGA)[6] usually are good choices, they fail when calculating strongly correlated electron systems such as that present in transition-metal compounds. In those cases, orbital-dependent methods like LDA + U (Ref. 7) or hybrid functionals are used. A comparison of band gap calculations using these different exchange-correlation functionals and experimental results is given in Ref. 8. There, the calculated density of states (DOS) of NiO is also compared with x-ray photoemission (XPS) and bremsstrahlung isochromat spectroscopy (BIS) measurements reported in Ref. 9.

Recently, a modified Becke-Johnson (TB-mBJ) exchange potential was tested for the calculation of band gaps.[10,11] This potential reads

$$v_{x,\sigma}^{\text{TB-mBJ}}(\boldsymbol{r}) = c\, v_{x,\sigma}^{\text{BR}}(\boldsymbol{r}) + (3c-2)\frac{1}{\pi}\sqrt{\frac{5}{6}}\sqrt{\frac{t_\sigma(\boldsymbol{r})}{\rho_\sigma(\boldsymbol{r})}}, \quad (1)$$

where $\rho_\sigma = \sum_{i=1}^{N_\sigma} |\psi_{i,\sigma}|^2$ denotes the electron density and $t_\sigma = (1/2)\sum_{i=1}^{N_\sigma} \nabla\psi_{i,\sigma}^* \nabla\psi_{i,\sigma}$ is the kinetic-energy density.

$$v_{x,\sigma}^{\text{BR}}(\boldsymbol{r}) = -\frac{1}{b_\sigma(\boldsymbol{r})}\left(1 - e^{-x_\sigma(\boldsymbol{r})} - \frac{1}{2}x_\sigma(\boldsymbol{r})e^{-x_\sigma(\boldsymbol{r})}\right) \quad (2)$$

is the Becke-Roussel potential,[12] which was designed to model the Coulomb potential created by the exchange hole. x_σ is calculated using a nonlinear equation[12] with ρ_σ, $\nabla\rho_\sigma$, $\nabla^2\rho_\sigma$, and t_σ, while b_σ is determined using $b_\sigma = [x_\sigma^3 e^{-x_\sigma}/(8\pi\rho_\sigma)]^{1/3}$. The value of parameter c in Eq. (1) is calculated using

$$c = \alpha + \beta\left(\frac{1}{V_{\text{cell}}}\int_{\text{cell}}\frac{|\nabla\rho_\sigma(\boldsymbol{r}')|}{\rho_\sigma(\boldsymbol{r}')}d^3r'\right)^{1/2}, \quad (3)$$

where V_{cell} is the unit cell volume and $\alpha = -0.012$ and $\beta = 1.023\ \text{bohr}^{1/2}$ are parameters determined according to a fit to experimental values.[11] The original Becke-Johnson potential is recovered by setting $c = 1$. It is notable that the TB-mBJ potential cannot be obtained as a functional derivative of an exchange functional (there is no E_x such that $v_{x,\sigma}^{\text{TB-mBJ}} = \delta E_x/\delta\rho_\sigma$).[11,13] Therefore, this potential should not be used for the calculation of forces, the comparison of total energies, or the optimization of the geometry.[10,11,13,14]

The Becke-Johnson potential and modified versions of it (including the TB-mBJ potential used in the present work) have been utilized by several groups so far. For example, Singh tested the prediction of the TB-mBJ potential for the electronic structure and magnetic properties of condensed systems.[15] Kim *et al.*[16] applied the TB-mBJ potential on III-V semiconductors, while Pittalis *et al.*[17] extended the Becke-Johnson potential for use on two-dimensional systems. Räsänen *et al.*[18] provided a different correction of the Becke-Johnson potential, which Oliveira *et al.*[19] compared to experiments for atoms, molecules, and atomic chains.

When investigating the effects of a modified Becke-Johnson potential, the focus usually lies on comparing the band structure, density of states, and band gaps, but magnetic moments have also been analyzed successfully.[11,14] In comparison to Perdew-Burke-Ernzerhof (PBE) calculations, the TB-mBJ potential gives much better values compared to experimental magnetic moments.[11,14] The experimental values for NiO are 1.64–1.9μ_B (Ref. 8) compared to 1.39μ_B for PBE and 1.76μ_B for TB-mBJ.

In Ref. 11, the resulting DOS, obtained with calculations using the TB-mBJ potential, is compared to XPS/BIS measurements from Ref. 9. In Fig. 2 of Ref. 11, the calculated valence band DOS is compared with O K and Ni L x-ray emission spectroscopy. From there, it can be seen that the

TB-mBJ calculation gives the correct positions of Ni d and O p bands with respect to each other. The TB-mBJ potential gives results in good agreement with experimental values that are similar to those produced by more sophisticated methods but at much lower computational costs.[11]

As NiO is a 3d transition-metal oxide, it is an ideal example to demonstrate the effects of different exchange-correlation potentials. In this work we calculate the oxygen K edge ELNES of NiO using different models for the exchange-correlation functional and compare it to experimental measurements. The focus lies on the oxygen K edge, as DFT is not sufficient for the calculation of the Ni $L_{2,3}$ edge and one would need to solve the Bethe-Salpeter equation instead.[20]

II. DENSITY OF STATES

The simulations were performed using the full-potential augmented-plane-wave code WIEN2K,[21] version 10.1. The in-

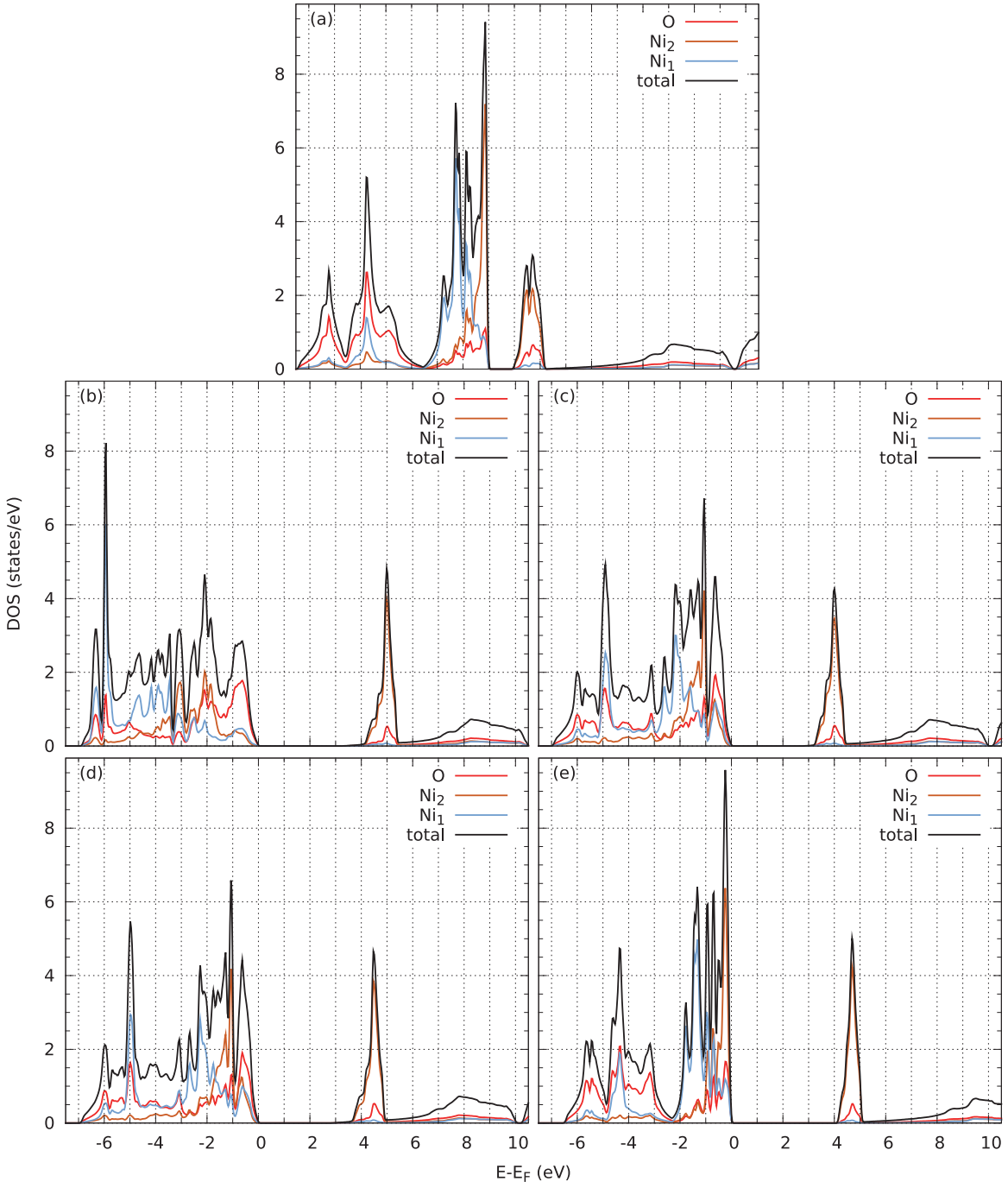

FIG. 1. (Color online) Total DOS calculated using different models for the exchange-correlation potential. The energy is plotted with respect to the Fermi energy E_F. The total atomic DOS is marked in different colors. The labels Ni_1 and Ni_2 refer to majority and minority spin of Ni atoms in the spin-polarized calculation. (a) PBE. (b) LDA + U. (c) Hybrid potential B3PW91. (d) Hybrid potential PBE0. (e) Modified Becke-Johnson potential TB-mBJ.

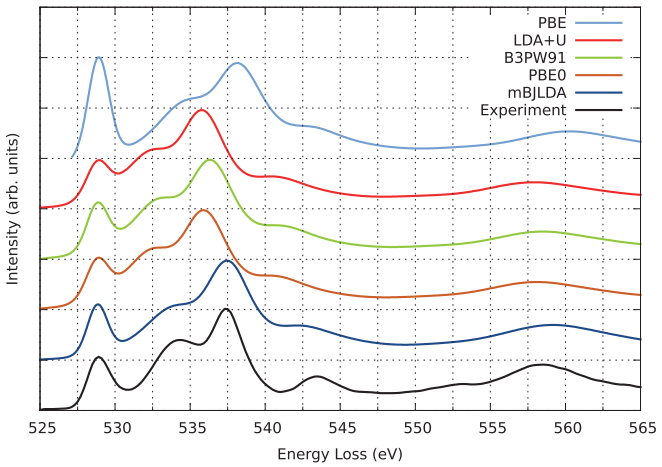

FIG. 2. (Color online) Oxygen K edge ELNES calculated using different exchange-correlation functionals compared to the experimental spectrum. The spectra are shifted vertically for better visibility.

put for structure type, lattice parameters, and atomic positions to calculate antiferromagnetic NiO is shown in Table I. All calculations were performed using 2000 k points, similar to the simulations reported in Ref. 23. A plane-wave cutoff parameter $R_{\mathrm{MT}}K_{\mathrm{max}}$ of 7 was used. The atomic sphere radii of both Ni atoms were 2.09 and 1.85 a.u. for the O atom, which corresponds to 0.111 and 0.098 nm, respectively. All calculations were performed using spin polarization. Simulations were done systematically with the generalized gradient approximation reported by Perdew, Burke and Ernzerhof,[6] LDA + U (Ref. 7), two different local[8,24] hybrid potential methods [PBE0 (Refs. 25 and 26) and B3PW91 (Ref. 27)], and TB-mBJ[11] as implemented self-consistently in the WIEN2K package. After convergence of the self-consistent field (SCF) cycle the DOS and ELNES spectra were calculated in order to compare them with experimental values.

The total DOS calculated using the PBE method is shown in Fig. 1(a). It can be seen that the PBE method gives a band gap of about 1 eV. Thus, it severely underestimates the experimental band gap of 4.0–4.3 eV (see Ref. 8, references therein and Ref. 9).

In Fig. 1(b) the total DOS calculated using the LDA + U method is shown. As in Ref. 8 the value for U_{eff} was 7.05 eV = 0.52 Ry. With a calculated band gap width of 3.2 eV a significant improvement is evident. Also the general shape of the valence band states is different compared to the PBE calculation and to experimental data.[8,9]

The total DOS calculated with two different hybrid potential methods, namely, the B3PW91 and PBE0 functionals, is shown in Figs. 1(c) and 1(d). It can be seen that in both cases the band gap width of 2.8 eV still underestimates the experimental values. Both plots are very similar, with only slight differences in the valence band and the unoccupied Ni 3d states between Fermi level E_F and $E_F + 5$ eV.

Figure 1(e) shows the calculated total DOS using the modified Becke-Johnson potential which is used together with LDA (mBJLDA) for the correlation. It can be seen that this simulation method results in a band gap of 4.16 eV.

Thus, from all the potentials applied in this work, the modified Becke-Johnson potential is the only one which gives a band gap width similar to the experimentally acquired one. The DOS of the valence band is very similar to the PBE and the hybrid potential simulations and also in agreement with XPS/BIS measurements.[9] Compared to the LDA + U simulation the structure of the valence band is clearly different, which is mainly due to differences in the Ni 3d DOS. The unoccupied Ni 3d states are shifted to higher energies in the mBJLDA calculation, causing a more realistic value of the band gap.

As the electron energy loss spectra depend on the unoccupied density of states (for calculation methods see, e.g., Ref. 28), attention has to be directed to the structures above the Fermi level. In all calculation methods the shapes of these structures are similar, but peak positions and relative intensities are different. This gives rise to different near-edge structures in the energy loss spectra, which will be discussed in the next section.

TABLE I. Input data for the calculation of antiferromagnetic NiO using WIEN2K according to Ref. 22. Atom positions are given in local coordinates of the rhombohedral unit cell.

Lattice	Lattice parameters	Atom positions
R	$a = b = 2.966163$ Å	Ni_1: $x = 0$, $y = 0$, $z = 0$
	$c = 14.531171$ Å	Ni_2: $x = \frac{1}{2}$, $y = \frac{1}{2}$, $z = \frac{1}{2}$
		O: $x = \pm\frac{1}{4}$, $y = \pm\frac{1}{4}$, $z = \pm\frac{1}{4}$

III. ENERGY LOSS NEAR-EDGE STRUCTURE

ELNES spectra were calculated using the program TELNES.[21,29,30] All the following calculations were done using 200 keV primary beam energy, a collection semiangle of 10.0 mrad, and a convergence semiangle of 0.01 mrad. An energy window of 50 eV and a step size of 0.05 eV were used. A value of 1.4 eV was taken for the spectrometer broadening according to the full width at half maximum (FWHM) of the experimentally measured zero-loss peak (ZLP). A Lorentzian broadening for core and valence lifetimes was also applied.

In Fig. 2 a comparison of the oxygen K edge ELNES calculated with different exchange-correlation functionals is shown. As the oxygen K edge EELS probes the excitation of 1s electrons, dipole-allowed transitions are those into p states. Therefore the shape of the ELNES should resemble the p-projected DOS above the Fermi level, except for effects like broadening. Other contributions like monopole or quadrupole transitions can be neglected as they are much smaller than the dipole-allowed contributions.[31,32]

The hole left by the excited core electron changes the electronic structure of the crystal. However, the effect of this core-hole is not always visible.[33] Usually a core-hole calculation with supercells has to be performed to take these changes into account and to see wether it has any effect on the calculated spectra. For the oxygen K edge of NiO considering the core-hole does not modify the resulting spectra significantly.[34] However, we still investigated its effect in the mBJLDA calculation using 48-atom supercells and taking either a full or half a core-hole into account. The excited electron was not added to the valence states since this would

(unphysically) occupy a Ni *d* state, but it was added as uniform charge in the unit cell (these high O *p* states are expected to be very diffuse states).

An experimental spectrum is also shown in Fig. 2. It was acquired using a FEI TECNAI G^2 20 microscope with a LaB_6 cathode, operated at 200 kV and equipped with a GATAN GIF 2001 energy filter. All the spectra were aligned at the first peak. This was done because a WIEN2K and TELNES calculation does not give absolute energy values. The energies are rather given with respect to the Fermi level, which is set to the valence band maximum. It is evident that by using different functionals a change in peak positions and relative intensities can be seen. This results from differences in the oxygen *p* DOS above the Fermi energy, which is shown in Fig. 3.

It is clear from Fig. 2 that although the shape of the spectra is reproduced well, the peak positions do not match the experiment very well when using PBE, LDA + U, or the hybrid potentials. Furthermore, using LDA + U and the hybrid functional PBE0, the relative intensity of the first peak is underestimated; using the hybrid exchange-correlation functional B3PW91, it is minimally overestimated, whereas using the GGA functional, the peak intensity is far overestimated.

All parameters in a WIEN2K calculation which can affect the results (*k* mesh, plane-wave cutoff) have been converged, but in agreement with what is reported in Ref. 34, neither changes in those parameters nor performing simulations including spin-orbit interaction improves the agreement with experiment.

The calculation of the actual values of $U_{\text{eff}} = U - J$ (with U and J being the Coulomb and exchange interaction) is discussed in Ref. 23. Following this discussion, in Fig. 4 oxygen *K* edge ELNES calculations for different values of U_{eff}, ranging from 0.25 to 0.55 Ry, are compared.

With increasing U_{eff} the relative intensity of the first peak decreases, leading to a better agreement with the experiment. However, at the same time the peak positions are changed, and therefore the agreement with experimental spectra is getting worse.

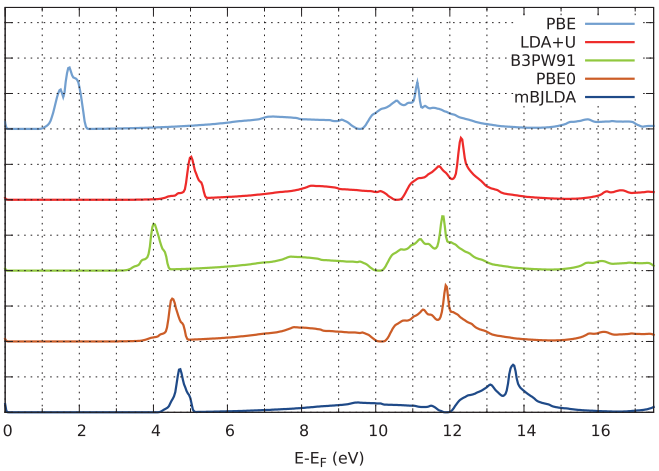

FIG. 3. (Color online) Comparison of the O *p*-projected DOS above the Fermi level calculated using different exchange-correlation functionals. The spectra are shifted vertically for better visibility.

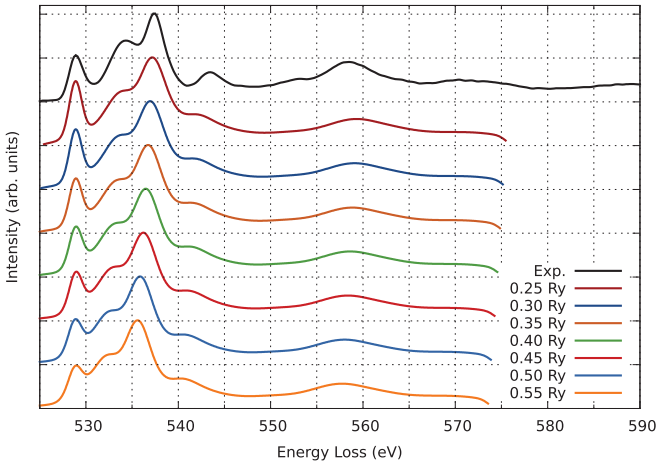

FIG. 4. (Color online) Oxygen *K* edge ELNES calculated using the LDA + U functional and different values of U_{eff}, ranging from 0.25 to 0.55 Ry, compared to the experimental spectrum. The spectra are shifted vertically for better visibility.

In Fig. 2, the experimentally measured oxygen *K* edge ELNES is compared to the simulation using the TB-mBJ potential. It can be seen that the peak positions and the relative intensities are reproduced very well. The differences to the experimental spectrum at the peaks at 534 and 543 eV lead to the assumption that these parts in the unoccupied DOS are still underestimated. This gives rise to the fact that these peaks are not emphasized enough when calculating the broadening. This can be seen in Fig. 5, where a comparison of the oxygen *p* DOS calculated using the modified Becke-Johnson potential and the broadened and the unbroadened spectra are shown. For more details on calculating the broadening see for example Refs. 35 and 36.

In Fig. 6 mBJLDA calculations using half a core-hole and a full core-hole are compared to the calculation without a core-hole and to the experimental spectrum. When using half

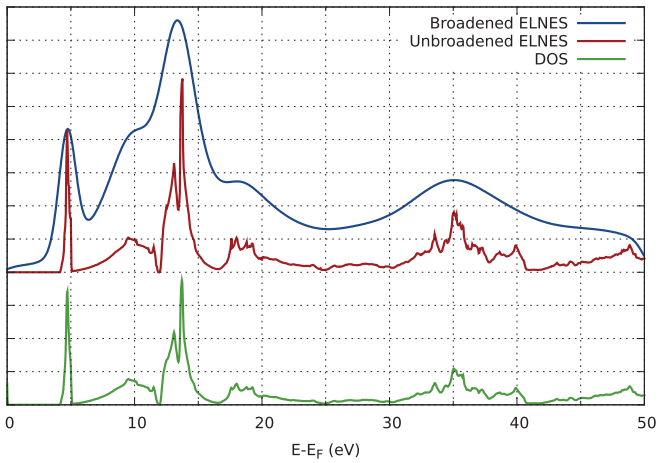

FIG. 5. (Color online) Broadened and unbroadened O *K* edge ELNES compared to O p-projected DOS, calculated using the TB-mBJ potential. For the ELNES the energy beyond the edge onset is plotted, while for the DOS it is the energy above the Fermi-level. The spectra are shifted vertically for better visibility.

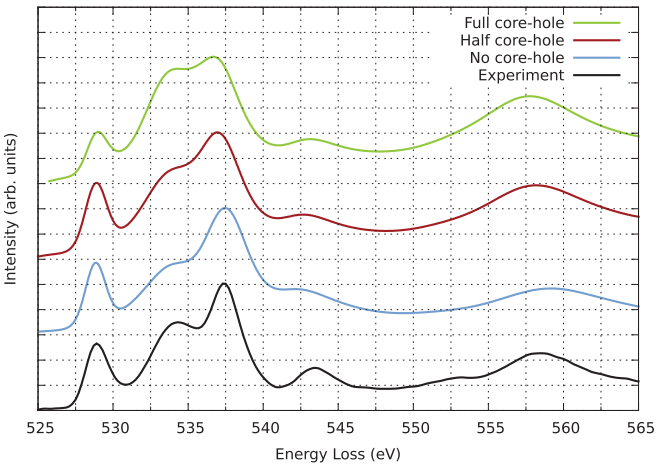

FIG. 6. (Color online) Comparison of the oxygen K edge ELNES mBJLDA calculations using a full core-hole, half a core-hole, no core-hole and the experimental spectrum. The spectra are shifted vertically for better visibility.

a core-hole the peaks at 537.5 and 558 eV are shifted to lower values of the energy loss, while the peak at 543 eV is shifted to higher values. These shifts are increased when using a full core-hole. In both core-hole calculations the peak at 543 eV is more pronounced than in the one without a core-hole. The relative intensity of the first peak is minimally overestimated with the partial core-hole, while it is underestimated when using a full core-hole. Compared to the main peak, the relative intensity of the peak at 534 eV fits best to the experimental spectrum when using half a core-hole. Considering all these details, the calculation using a partial core-hole fits best to the experimentally acquired spectrum. This is in agreement with what is reported in Ref. 37 and the concept of Slater's transition state.[38]

As the calculations using the modified Becke-Johnson potential show the best agreement with the experimental spectra, it is of interest to mention which part of this potential is responsible for the improvement compared to other exchange-correlation functionals. In addition to a term which models the Coulomb potential of the exchange hole [Eq. (2)], the Becke-Johnson potential includes a term with the kinetic-energy density [second term in Eq. (1)].[10] The modified Becke-Johnson potential furthermore incorporates a parameter which changes the weight between these two terms [Eq. (3)].[11] Its value is determined from the electron density for each material during the calculation.

In Ref. 14 the advantages and also the limits of this modified Becke-Johnson potential when calculating band gaps, magnetic moments, and the electric field gradient are investigated in more detail. This is done by studying the differences of the electron densities of different materials when using the PBE method and the modified Becke-Johnson potential. In Ref. 14 it is shown that this kinetic-energy density term [second term in Eq. (1)] is responsible for most of the changes, as it increases the energy of the unoccupied states and changes the corresponding band structure. Due to the weighting parameter c [Eq. (3)], on the other hand, the modified Becke-Johnson potential gives good results for a wide variety of different materials.

IV. CONCLUSION

Simulations of the DOS and oxygen K edge energy loss spectra of NiO were conducted using different models of the exchange-correlation potential. Whereas the PBE and hybrid potential methods give unsatisfactory results for the band gap as well as the ELNES spectra, the modified Becke-Johnson potential is in good agreement with experimental results. LDA + U improves the value of the calculated band gap, but the shape of the occupied DOS does not fit the experimental data. The modified Becke-Johnson potential renders a more realistic density of states due to a kinetic-energy density term and a weighting parameter which is determined for each material during the calculation. Furthermore, there is no need to tune calculation parameters. Another advantage of this exchange-correlation potential is that it is as cheap in the sense of computational costs as LDA or GGA methods.

ACKNOWLEDGMENTS

W.H. and P.S. acknowledge financial support from the Austrian Science Fund (FWF), Grant No. I543-N20. W.H. thanks Stefan Löffler and Michael Stöger-Pollach for fruitful discussions and support. P.B. was supported by the FWF (SFB 41, ViCoM).

*walid.hetaba@tuwien.ac.at

[1] R. F. Egerton, *Electron Energy-Loss Spectroscopy in the Electron Microscope*, 2nd ed. (Plenum, New York, 1996).
[2] R. F. Egerton, Rep. Prog. Phys. **72**, 016502 (2009).
[3] P. Hohenberg and W. Kohn, Phys. Rev. **136**, B864 (1964).
[4] W. Kohn and L. J. Sham, Phys. Rev. **140**, A1133 (1965).
[5] J. P. Perdew and Y. Wang, Phys. Rev. B **45**, 13244 (1992).
[6] J. P. Perdew, K. Burke, and M. Ernzerhof, Phys. Rev. Lett. **77**, 3865 (1996).
[7] V. I. Anisimov, I. V. Solovyev, M. A. Korotin, M. T. Czyżyk, and G. A. Sawatzky, Phys. Rev. B **48**, 16929 (1993).
[8] F. Tran, P. Blaha, K. Schwarz, and P. Novák, Phys. Rev. B **74**, 155108 (2006).
[9] G. A. Sawatzky and J. W. Allen, Phys. Rev. Lett. **53**, 2339 (1984).
[10] F. Tran, P. Blaha, and K. Schwarz, J. Phys. Condens. Matter **19**, 196208 (2007).
[11] F. Tran and P. Blaha, Phys. Rev. Lett. **102**, 226401 (2009).
[12] A. D. Becke and M. R. Roussel, Phys. Rev. A **39**, 3761 (1989).
[13] A. P. Gaiduk and V. N. Staroverov, J. Chem. Phys. **131**, 044107 (2009).
[14] D. Koller, F. Tran, and P. Blaha, Phys. Rev. B **83**, 195134 (2011).
[15] D. J. Singh, Phys. Rev. B **82**, 205102 (2010).

[16]Y.-S. Kim, M. Marsman, G. Kresse, F. Tran, and P. Blaha, Phys. Rev. B **82**, 205212 (2010).
[17]S. Pittalis, E. Räsänen, and C. R. Proetto, Phys. Rev. B **81**, 115108 (2010).
[18]E. Räsänen, S. Pittalis, and C. R. Proetto, J. Chem. Phys. **132**, 044112 (2010).
[19]M. J. T. Oliveira, E. Räsänen, S. Pittalis, and M. A. L. Marques, J. Chem. Theory Comput. **6**, 3664 (2010).
[20]R. Laskowski and P. Blaha, Phys. Rev. B **82**, 205104 (2010).
[21]P. Blaha, K. Schwarz, G. K. H. Madsen, D. Kvasnicka, and J. Luitz, WIEN2K, an augmented plane wave + local orbitals program for calculating crystal properties, Technische Universität Wien, Vienna, 2001.
[22]*Pearson's Handbook of Crystallographic Data for Intermetallic Phases*, 2nd ed., edited by P. Villars and L. Calvert (ASM International, Materials Park, Ohio, 1996).
[23]T. Cai, H. Han, Y. Yu, T. Gao, J. Du, and L. Hao, Phys. B **404**, 89 (2009).
[24]This means that the Hartree-Fock exchange is applied only to the 3*d* electrons inside the Ni atomic spheres.
[25]M. Ernzerhof and G. E. Scuseria, J. Chem. Phys. **110**, 5029 (1999).
[26]C. Adamo and V. Barone, J. Chem. Phys. **110**, 6158 (1999).
[27]A. D. Becke, J. Chem. Phys. **98**, 5648 (1993).
[28]M. Nelhiebel, P.-H. Louf, P. Schattschneider, P. Blaha, K. Schwarz, and B. Jouffrey, Phys. Rev. B **59**, 12807 (1999).
[29]M. Nelhiebel, Ph.D. thesis, École Centrale Paris, 1999 .
[30]K. Jorissen, Ph.D. thesis, Universiteit Antwerpen, 2007 .
[31]C. Hébert, Micron **38**, 12 (2007).
[32]S. Löffler, I. Ennen, F. Tian, P. Schattschneider, and N. Jaouen, Ultramicroscopy **111**, 1163 (2011).
[33]V. Mauchamp, M. Jaouen, and P. Schattschneider, Phys. Rev. B **79**, 235106 (2009).
[34]L. V. Dobysheva, P. L. Potapov, and D. Schryvers, Phys. Rev. B **69**, 184404 (2004).
[35]D. A. Muller, D. J. Singh, and J. Silcox, Phys. Rev. B **57**, 8181 (1998).
[36]P. Moreau, F. Boucher, G. Goglio, D. Foy, V. Mauchamp, and G. Ouvrard, Phys. Rev. B **73**, 195111 (2006).
[37]J. Luitz, M. Maier, C. Hébert, P. Schattschneider, P. Blaha, K. Schwarz, and B. Jouffrey, Eur. Phys. J. B **21**, 363 (2001) .
[38]J. C. Slater, *Quantum Theory of Molecules and Solids*, Vol. 4, *The Self-Consistent Field for Molecules and Solids* (McGraw-Hill, New York 1974) .